ACS APPLIED MATERIALS & INTERFACES

Research Article

www.acsami.org

Modulating Particle Adhesion with Micro-patterned Surfaces

Cong Yu,[†] Jianwei Ma,[†] Jiangnan Zhang,[‡,∥] Jun Lou,[‡] Donghui Wen,[§] and Qilin Li*[,†]

[†]Department of Civil and Environmental Engineering, Rice University, Houston, Texas 77005, United States

[‡]Department of Materials Science and Nanoengineering, Rice University, Houston, Texas 77005, United States

[§]College of Environmental Sciences and Engineering, Peking University, Beijing 100871, China

Supporting Information

ABSTRACT: We report the first experimental study on the modulation of adhesion force distribution by surface micro-patterns and its impact on particle attachment. The effect of substratum topography on particle adhesion was evaluated using well-defined microscopic surface patterns consisting of orthogonal arrays of cuboid pillars or pits with different sizes and spacing fabricated by the conventional photolithography and reactive ion etching (RIE). Adhesion of carboxyl modified poly(styrene-*co*-acrylic-acid) particles of 6 μm in diameter under favorable deposition conditions was found to be markedly lower on all the micro-patterned surfaces compared with that on the smooth control surface, and particle adhesion depended on the characteristic dimensions of the surface micro-structures relative to the particle size. Particle adhesion was minimal when the pillar cross-sectional dimension was below a critical value close to the diameter of the particle while the spacing between pillars was less important. Meanwhile, particles adhered displayed unique distribution on the micro-patterned surfaces. The majority of particles preferentially adhered on or close to the edge of the pillars (in the valley). Atomic force microscopy measurements using a colloidal probe revealed that the surface features strongly modulated the spatial and probability distribution of adhesion forces on the micro-patterned surfaces. Micro-sized pillars changed the adhesion force probability distribution from monomodal to bimodal, with significantly reduced maximum adhesion force. This was hypothesized to be responsible for the reduced total particle adhesion.

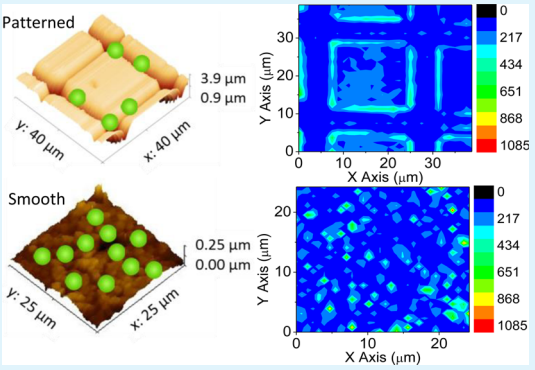

KEYWORDS: *surface topography, particle adhesion, micro-pattern, adhesion force mapping, atomic force microscopy*

INTRODUCTION

Adhesion of biological (e.g., bacterial, algal, and mammalian cells) and nonbiological particles on surfaces is an important process that affects numerous applications including medical implants, tissue engineering, semiconductor manufacturing, surface coating, separation processes, and fouling control in aquatic systems.[1] In order to tailor surface properties to control (enhance or inhibit) particle deposition and adhesion, a thorough understanding of how material surface morphology and chemistry affect particle adhesion is necessary.

Particle adhesion on surfaces is a complex process influenced by the characteristics of the particle, the solution condition, and the physicochemical properties of the substrate surface including electrical properties, hydrophobicity, and surface morphology.[2,3] The roles of surface charge and hydrophobicity are relatively well understood and are commonly used to explain the observed adhesion behaviors as well as to manipulate particle adhesion.[4] The effect of surface morphology, however, is less understood. This is largely due to the random nature of surface roughness features, which is poorly characterized. The commonly used characterization parameters such as average and root mean square roughness do not provide specific information on the size, shape, and distribution of surface features.[5]

In the past few decades, accumulating evidence of biological and nonbiological particles responding to topographical cues has emerged in studies of engineered surfaces with well-defined surface topographical features, which enables systematic investigation of the interactions between particles and surface features.[5−7] It is well established that mammalian cells respond to micro- and nano-sized engineered patterns.[8] Selective adhesion as well as changes in cell orientation and nucleus shape has been reported.[9−11] The impact of surface topographical cues on smaller particles including non-biological colloids and bacteria is less understood.[6] Darbha et al.[7] reported increased attachment of latex particles (0.3−2 μm in diameter) on pit-patterned silicon surfaces under flow conditions, and the increase in particle deposition was greater for smaller particles. Studies on bacterial adhesion have reported surface topographical structures that enhance,[12,13] reduce,[14−21] or have no effect[21] on bacterial adhesion relative to smooth surfaces

Received: February 11, 2014
Accepted: April 28, 2014
Published: April 28, 2014

depending on the size of the surface structures and the bacterial type. Medilanski et al.[15] showed reduced adhesion of four bacterial strains on surfaces with parallel channels with an average width of 0.7 μm, but enhanced adhesion on surfaces with wider grooves. Using pillar-patterned polydimethylsiloxane (PDMS) surfaces, Hou et al.[16] also demonstrated that a critical surface feature size existed: square-shaped pillars smaller than the critical size (20 μm × 20 μm) led to decreased *E. coli* biofilm formation; for all pillar sizes, adhesion preferentially occurred in the valleys (5−100 μm). Hsu et al.[19] studied bacterial attachment on patterned silicon substrate with pits of 27 to 32 nm in depth with circular (500 nm diameter and 200 nm spacing) or rounded rectangular (1 × 1.5 μm, spacing 2 μm or 1 × 2 μm, spacing 500 nm) cross sections. All patterns significantly reduced attachment of Gram-negative bacteria, *E. coli* and *P. fluorescens* but not the Gram-positive bacterium, *L. innocua*, and the effect of pit shape was not obvious. The study on micro-sized cone patterns by Perni et al.[21] showed that cones with diameters of 25 or 30 μm enhanced bacterial adhesion while 20 or 40 μm inhibited adhesion and the spacing between cones (4−13 μm) showed little effect. The bacterial cells preferentially adhere in the valleys near the surface features comparing to random distribution on control surface. Scheuerman et al.[22] studied the effect of micro-sized grooves (10 μm deep and 10−40 μm wide) on adhesion of three strains of bacteria and hydrophilic, negatively charged microspheres (1 μm) under flow conditions. Under the conditions tested, there was no attachment of the microspheres, but significant bacterial attachment was observed; the bacterial deposition rate was governed by the transport from the bulk solution to the substratum, which was independent of the width of the grooves. The grooves, however, strongly impacted the distribution of cells, which preferentially attached on the downstream edge of the grooves, indicating that the grooves sheltered the cells from hydraulic shearing.

Two physicochemical mechanisms have been proposed to explain the observed effects. The surface features could alter the hydrodynamic conditions near the surface, for example, shielding particles from hydraulic shear,[22] and change the interaction energy between the particle and the surface. A number of theoretical studies have investigated the impact of surface morphology on the DLVO (Derjaguin−Landau−Verwey−Overbeek) interaction energy between a spherical particle and a flat surface. Hemispherical surface features were found to generally reduce the average particle-surface DLVO interactions, repulsive or attractive, by increasing the separation distance between the particle and the surface;[23−25] local particle-surface interaction potential, however, can be either increased (by hemispherical pit) or decreased (by hemispherical protrusion) comparing to planar surface.[23] Martines et al.[26] showed the total DLVO interaction energy between a 10 μm spherical particle and patterned surfaces with nano-sized cylindrical pillars/pits or hemispherical pillars relative to that for the smooth control was a complex function of the type (pillars vs pits) and dimensions of surface features as well as ionic strength: All patterns reduced the secondary minimum depth; pillars reduced the energy barrier in all solution conditions while pits could either increase or reduce the energy barrier depending on the salt concentration; the energy barrier decrease with increased radius of curvature. For biological particles, the surface features can also trigger physiological changes relevant to cell adhesion (e.g., cell shape, number and size of surface appendages, and cell proteomics).[19,27−29]

These previous studies clearly demonstrate that surface patterns consisting of micrometer- or submicrometer-sized features strongly affect particle adhesion, and the effects depend on the shape and size of the surface features as well as the particle characteristics. However, the specific effect of surface feature size is unclear. Moreover, most of the previous experimental studies employed biological particles (i.e., microorganism cells), the attachment of which involves both physicochemical and biological interactions, making it difficult to understand specific mechanisms. The study reported here systematically examined the impact of surface micro-topography on physicochemical interactions involved in particle attachment utilizing model fluorescent particles and engineered surfaces with well-defined micro-topographic patterns and uniform surface chemistry. A series of orthogonal arrays of cuboid pillars or pits with different feature dimensions and spacing were fabricated by photolithography and RIE on silicon substrate. The particle adhesion on the patterned surfaces was characterized using fluorescence microscopy. Atomic force microscopy (AFM) utilizing a colloid probe was performed to directly measure the adhesion force between the particle and the patterned surfaces. The experimental results revealed the critical role that micro-scale surface features play in modulating particle attachment and the specific effect of surface feature size. To our knowledge, this is the first experimental study that clearly showed the modulation of adhesion force distribution by surface micro-patterns and its relation to particle attachment.

EXPERIMENTAL SECTION

Materials. Silicon wafers (500 ± 25 μm thickness; 100 mm diameter, (111) orientation) polished on one side were obtained from Addison Engineering, Inc. (San Jose, CA). Carboxyl modified poly(styrene-*co*-acrylic acid) (PSAA) green fluorescence microspheres of 6.0 μm in diameter (1.0% solids, Phosphorex, Inc., Hopkinton, MA) was used as model colloidal particles. The highly negatively charged carboxyl functionalized surface is representative of particulate organic matter and bacterial cells. The excitation and emission wavelengths of the fluorescent dye are 480 and 509 nm, respectively. The density of the carboxyl function groups is 6.02×10^7/sphere. The ζ-potential of the PSAA particles was measured using a Zetasizer Nano (Malvern Instruments Ltd., U.K.) in the background electrolyte solution used in the particle adhesion experiments (100 mM NaCl) at different pHs and the results are shown in Figure S1 in the Supporting Information.

Reagent-grade 190 proof ethanol (95%) was obtained from DECON Labs, Inc (King of Prussia, PA). Reagent-grade sodium chloride and hydrochloric acid (GR, ACS Grade, 37%) were obtained from Fisher Scientific (Pittsburg, PA). All solutions and suspensions were prepared using ultrapure water (≥18.1 MΩ cm) generated by an E-Pure system (Barnstead, Batavia, IL).

Micro-patterned Surface Fabrication. The silicon wafers were tailored to obtain small chips of 0.8 cm × 1.2 cm in size using a diamond-tipped scribe. The silicon chips were cleaned with Piranha solution at 110−130 °C for 60 min to remove organic contaminants, followed by purging with ultrapure nitrogen. Via standard photolithography method, orthogonal arrays of 1 mm × 1 mm patterns consisting of cuboidal microscopic features with square-shaped cross-section were fabricated on silicon chips. Briefly, the clean silicon chips were baked at 150 °C for 10−15 min. Two drops of S1813 photoresist (Microchem, Newton, MA) were spin-coated on the chips at 5000 rpm. After developed by a Mask Aligner (Suss Mask Aligner MJB4, mask manufactured by Fineline Imaging, Colorado Springs, CO), MF 319 developer (Microchem, Newton, MA) was used to remove the cross-linked photoresist on the silicon chip and the residual water was blown dry. A chromium layer of several micrometers in thickness was

sputtered on the chip surface (CRC-150 Sputter Coater, Torr International, NY, U.S.A.). The coated chip was boiled in Microposit Remover 1165 (Microchem, Newton, MA) at 100 °C for 60 min to remove the unexposed photoresist, leaving the chromium coating serving as the mask. A standard reactive ion etch (RIE, Minilock-Phantom III, Trion RIE, Clearwater, FL) procedure was then performed to obtain 2−3 μm in feature height. The chromium layer was removed by soaking the sample chips in a chromium etchant (CEP-200, containing 6% perchloric acid and 9% cerric ammonium nitrate) inside a hood for 60 seconds, thoroughly rinsing with DI water and blowing dry. To ensure homogeneous surface chemistry, the whole pattern surface was etched by a certain depth using the RIE procedure.

Two sets of patterns with pillars and pits of varied cross-section dimension (i.e., side length of the square-shaped cross-section) and edge-to-edge spacing were first fabricated to study the effect of micro-topography on particle attachment. The dimensions of the pattern features are listed in Table S1 in Supporting Information. To further evaluate the effect of feature size and spacing, two additional series of patterns containing cuboidal pillars with systematically varied pillar dimension or spacing were fabricated on a single silicon wafer: one series consisted of cuboidal pillars ranging from 5 to 40 μm in dimension with a fixed spacing of 5 μm; the other series consisted of cuboidal pillars of an identical dimension of 5 μm with the spacing between pillars varying from 5 to 40 μm. The pattern samples were thoroughly characterized by scanning electron microscopy (SEM, FEI Quanta 400, Hillsboro, OR), profilometry (Veeco DekTak 6M stylus profilometer, Plainview, NY), and X-ray photoelectron spectroscopy (XPS, PHI Quantera, Chanhassen, MN) for surface morphology, height profile, and surface chemical composition, respectively.

Particle Adhesion Experiments. Before each adhesion experiment, the silicon chips were thoroughly cleaned using the following protocol. The samples were first soaked in 2% Extran MA02 solution (EM Science, Gibbstown, NJ) for 2 h, followed by rinsing with ethanol and ultrapure water for five times. Subsequently, they were sonicated at room temperature in 2% RBS 35 (Pierce, Rockford, IL) detergent solution for 20 min and rinsed again with ethanol and ultrapure water. The samples were then soaked in the NOCHROMIX solution (GODAX Laboratories, Inc., Cabin John, MD) for 24 h, thoroughly rinsed with ultrapure water, and dried using particle free ultrapure nitrogen.

The clean patterned and control surfaces were placed side by side in the same well of a six-well tissue culture plate (Costar, Corning, NY) that was thoroughly cleaned and dried with particle-free nitrogen. Background electrolyte solution (5 mL) (100 mM NaCl with pH adjusted to 4 using HCl solution) was added into the well. The high salt concentration and low pH were chosen to create a favorable deposition condition. As shown in Figure S1 in Supporting Information, the PSAA particle surface ζ-potential was below −5 mV under this solution condition. The PSAA stock suspension (8.4×10^7 particles/mL) was sonicated for 15 min to ensure good dispersion and added into the test well to achieve a final concentration of 2×10^6/mL. The six-well plate was then wrapped in aluminum foil and shaken on an orbital shaker table (VWR OS-500, West Chester, PA) at 50 rpm at room temperature for 30 min. In order to avoid exposure to the air/water/solid interface, which causes strong surface forces that may disturb adhered particles, a rinsing protocol was developed without taking the samples out of the solution. In each rinse, the residual particle suspension was replaced with the background solution while keeping the samples submerged at all times; the plate was gently hand shaken horizontally in a circular motion for 2 min. This step was repeated 5 times. After the last rinse, a glass coverslip was put on the submerged test samples, and the samples were withdrawn for analysis. Adhesion experiments were repeated at least three times. All the apparatuses were extremely carefully cleaned to avoid any possible particle contamination.

After rinsing, the samples were imaged by an Axioplan 2 epifluorescence microscope (Carl Zeiss, Oberkochen, Germany). Images were acquired with a CoolSnap HQ camera (Photometrics, Tucson, Ariz) controlled by the Metamorph 7 imaging software (Molecular Devices Corporation, Sunnyvale, CA). Five images were acquired on each pattern and images were analyzed using the ImageJ software[30] to obtain the average particle number on each pattern.

AFM Adhesion Force Measurement. The adhesion force between the PSAA particle and the sample surfaces was quantified using AFM. The measurement employed a colloid probe prepared by attaching a PSAA particle to a silicon AFM probe (PPP-NCH-W, spring constant = 0.44 N/m, NanoSensors, Neuchatel, Switzerland) with a 24 h epoxy (Hardman, Wilmington, CA) using a micro-manipulator (DC-3KS Rechts, Marzhauser, Germany). The colloid probe was examined under an optical microscope and stored in dark at 4 °C until use. Before use, the colloid probe was examined again by scanning the colloid probe on an AFM calibration surface consisting of sharp arrays of spikes to ensure no contamination on the colloid probe surface. The AFM cantilever was calibrated using a standard reference method,[31] and the measured spring constant was 0.44 N/m, consistent with the manufacturer's specification.

All AFM experiments were performed in a liquid cell filled with the background solution used in the adhesion experiment, that is, 100 mM NaCl with pH adjusted to 4 using HCl. In order to obtain spatial distribution of the adhesion force, the 40 μm × 40 μm scan area was divided into 32 by 32 subareas. A force versus distance (FD) curve was collected in each subarea, and the corresponding adhesion force was acquired from each FD curve.

RESULTS AND DISCUSSION

Characterization of the Micro-patterned Surface. The photolithography-RIE method was able to produce precise and reproducible micro-patterns with well-defined surface features and few defects (Figure 1a). As shown in Figure 1b, the actual

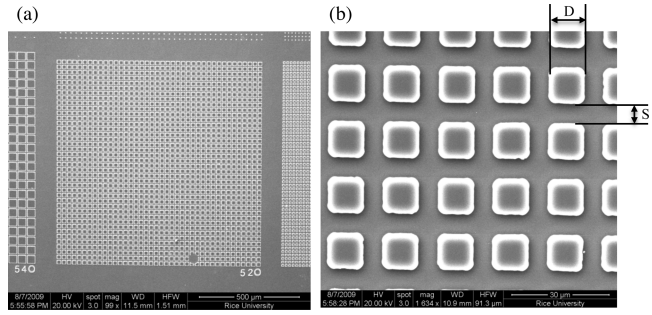

Figure 1. Representative SEM images of micro-patterned surfaces: (a) pillar dimension (D) = 20 μm, spacing (S) = 5 μm; (b) pillar dimension (D) = 12 μm, spacing (S) = 5 μm.

pillar dimension (D) and spacing (S) (11.89 and 5.05 μm, respectively, in this example) measured by SEM matched well with the design (12 μm and 5 μm for pillar dimension and spacing, respectively). Vertical profile of the patterns (see Figure S2 in Supporting Information for an example) showed good reproducibility of the micro-sized structures across the whole pattern surface. The pillars were about 2.7−2.8 μm in height. XPS analysis at various locations of the patterned surfaces found no chromium or other contaminants (Figure S3 in Supporting Information). Surface chemistry was uniform across the pattern surface, which ensured that any variation in particle deposition/adhesion was due to the difference in surface topography.

PSAA Particle Adhesion on Patterned Surfaces. Particle adhesion was first investigated using patterned surfaces with pillar or pit dimension significantly larger than the particle size. Results are shown in Figure 2. All patterns tested exhibited lower particle adhesion than the smooth control surface (red

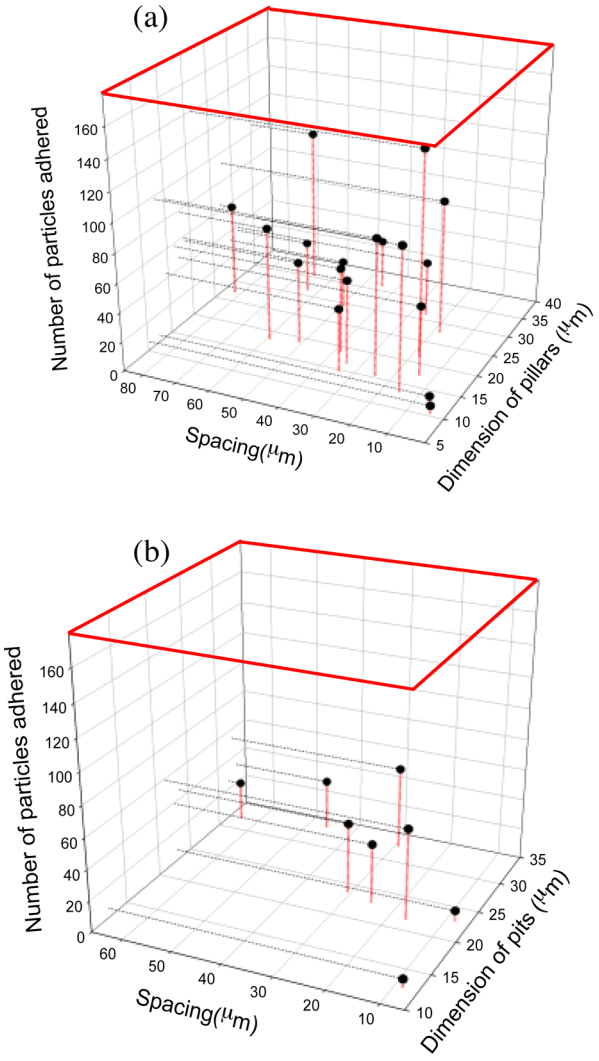

Figure 2. Particle adhesion on patterned surface with (a) pillars and (b) pits larger than particle diameter (The top surface outlined in red indicates the particle adhesion on the smooth control surface).

square on top). More importantly, particle adhesion in general decreased with decreasing feature dimension and spacing.

Particles attached on the smooth control surface were randomly distributed. On the patterned surfaces, however, their distribution was strongly influenced by the surface features (Figure 3). On pillar patterns with spacing much larger than the particle size, almost all particles adhered close to the wall of the

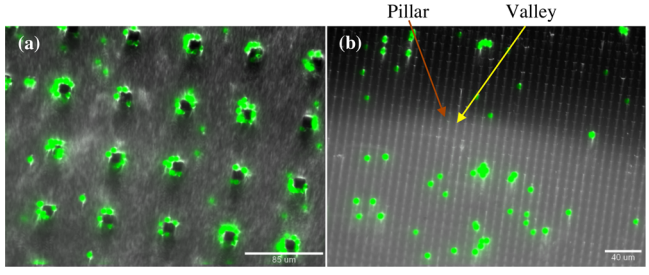

Figure 3. PSAA particle adhesion on two different pillared patterns (a) pillar dimension = 11.76 μm, spacing = 54.66 μm (scale bar is 85 μm); (b) pillar dimension = 8.36 μm, spacing = 3.61μm (scale bar is 40 μm).

pillars with very few on the pillar top or in the valleys, even though vast accessible surface area was available in the valleys (Figure 3a). When the spacing between pillars was similar to or smaller than the particle size, few particles attached and they randomly distributed over the valleys (Figure 3b).

In order to better understand the effect of surface feature size and spacing on particle adhesion, experiments were performed using pillar patterns with systematically varied spacing or feature dimension. The particle attachment results are summarized in Figure 4. Again, all patterned surfaces exhibited

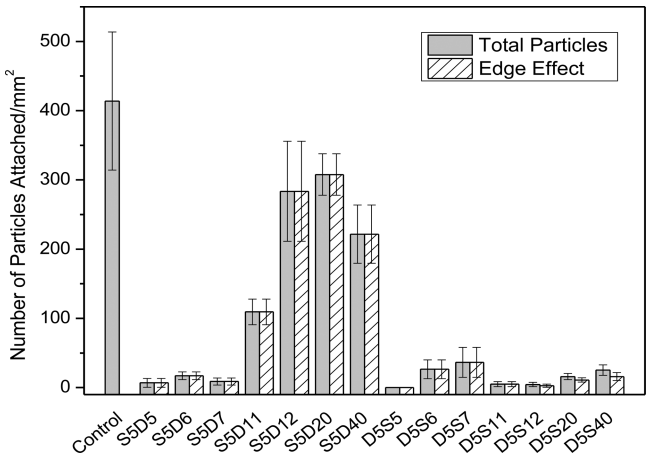

Figure 4. Number of colloidal particles attached to two series of pillar patterns (total particles) with systematically varied pillar dimension (D) or spacing (S) and only to the edge (edge effect).

markedly lower particle adhesion than the smooth control surface. Particle adhesion was minimum when the pillar dimension was kept between 5 and 7 μm, despite the wide range of spacing (5 to 40 μm) tested. The number of attached particles increased significantly as the dimension of the pillars increased beyond 7 μm. These results suggest that pillar size plays a critical role in particle adhesion on a micro-patterned surface; particle adhesion is minimized when the pillar size is smaller than or similar to the diameter of the particle. This is consistent with observations in a previous study that surface features of size similar to or smaller than the particles had more impact on adhesion.[32] Spacing between pillars, on the other hand, does not seem to be a critical factor except when the spacing was equal to or slightly larger than the particle diameter (i.e., spacing = 6 or 7 μm). Particle adhesion varied widely when the spacing was fixed at 5 μm while the pillar dimension was varied from 5 to 40 μm. When the pillar dimension was fixed at 5 μm, particle adhesion was the highest for spacing of 6 or 7 μm. This is attributed to the interaction of the particles with the pillar sidewalls.

Similar to that observed in Figure 3, in most cases, particles preferentially adhered on the edges of the pillars or in the valleys within close proximity to the pillars (Figures 5b–d), in contrast to the random distribution on the smooth control surface (Figure 5a), even for pillars as large as 40 μm, which provided plenty of accessible surface area for attachment on the pillar top. These particles were referred to as the "Edge Effect" particles in Figure 4, and accounted for over 62% of all particles attached on patterns with spacing from 12 to 40 μm and 100% on all other patterns.

Because surface patterning reduces the surface area accessible to particles, geometric analysis (Figure S4 in Supporting

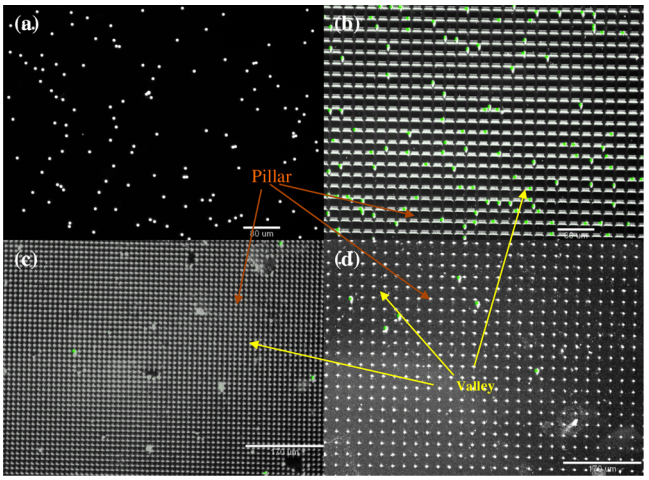

Figure 5. PSAA particle distribution on the (a) smooth control surface and pillar patterned surfaces: (b) pillar dimension = 20 μm, spacing = 5 μm (scale bar: 80 μm); (c) pillar dimension = 6 μm, spacing = 5 μm (scale bar = 170 μm); (d) pillar dimension = 5 μm, spacing = 20 μm (scale bar = 170 μm). Note: Because the light reflection changes with the pillar dimension and spacing, the pillars and the valley between them appear in different colors in different images.

Information) was done to calculate the frontal surface area available for particle adhesion. Figure 6a shows that the patterns can significantly reduce surface area accessible to particles. With a pillar dimension of 5 μm, the area accessible to the particles decreased with decreasing spacing due to the increasing number of pillars and hence the inaccessible area around them. With a spacing of 5 μm, only the area on the pillar tops was accessible to the particles. As a result, the accessible area decreased with decreasing pillar dimension. However, the measured particle adhesion showed no correlation with accessible area (Figure 6b). This suggests that the change in adhesion area is not responsible for the reduced particle attachment observed.

Adhesion Force Distribution on Patterned Surfaces. To understand the role of surface topography in the distribution of attached particles, the adhesion force on selected patterns and the smooth control was quantified with AFM using a PSAA colloid probe. As examined by optical microscope and AFM, the colloid tip surface was clean and no contamination of epoxy on the surface of the colloid probe was found (Figure S5 in Supporting Information).

Representative adhesion force maps over a 40 μm × 40 μm area on three pillar patterned surfaces and a 25 μm × 25 μm area on the smooth control surface as well as the 3-D surface topography images of the patterns are shown in Figure 7. The scanned area on the patterned surfaces included both pillars and valleys to represent the adhesion force over the whole pattern. While the adhesion force was randomly distributed on the smooth control surface (Figure 7d), it was strongly modulated by the micro-patterns (Figures 7e–g). Regardless of pattern dimensions, adhesion force was consistently the lowest on the pillar top among the accessible surface areas. This is in accordance with the observations in the particle adhesion experiments, when few particles are found to attach on the top of the pillars. For the pattern shown in Figure 7a and e, the colloidal probe was not able to reach the bottom of the valleys given the spacing (5 μm) between and the height (2.7–2.8 μm) of the pillars. As a result, the valley area showed essentially zero adhesion; the strongest adhesion was found along the edge of the pillars. This is consistent with the observed particle adhesion over the narrow valleys (Figure 5b). Patterns with spacing much larger than the particle size exhibited significantly higher adhesion force in valleys than that on the pillar top (Figure 7f and g). This is in accordance with the observation that particles only adhered in the valleys (Figure 5d) on these patterns. In the valleys, the area immediately adjacent to the pillar sidewalls had the lowest adhesion because the valley surface in this region is not accessible to the colloid probe.

Quantitative analysis of adhesion force distribution better elucidates the effect of surface micro-patterns on particle adhesion. The distribution density and cumulative probability of adhesion force on the smooth control and selected pillar patterns are shown in Figure 8. The adhesion force on the smooth control surface followed a mono-modal distribution close to Gaussian but with an extended tail in the high adhesion force range. This is consistent with the random distribution of particles on the control surface (Figure 5a). All patterned surfaces significantly changed the adhesion force distribution, with a notable increase in frequency in the 0–20 nN range. This is attributed to the inaccessible area in the valleys and the low adhesion area on the pillar tops (schematics in Figure S4 in Supporting Information). When pillar size was decreased, a bimodal distribution of adhesion force developed, which was clearly seen on the patterns with a pillar size of 5 μm. The occurrence of the second mode seems to depend on the spacing. A spacing of 12 μm (twice the particle size) resulted in

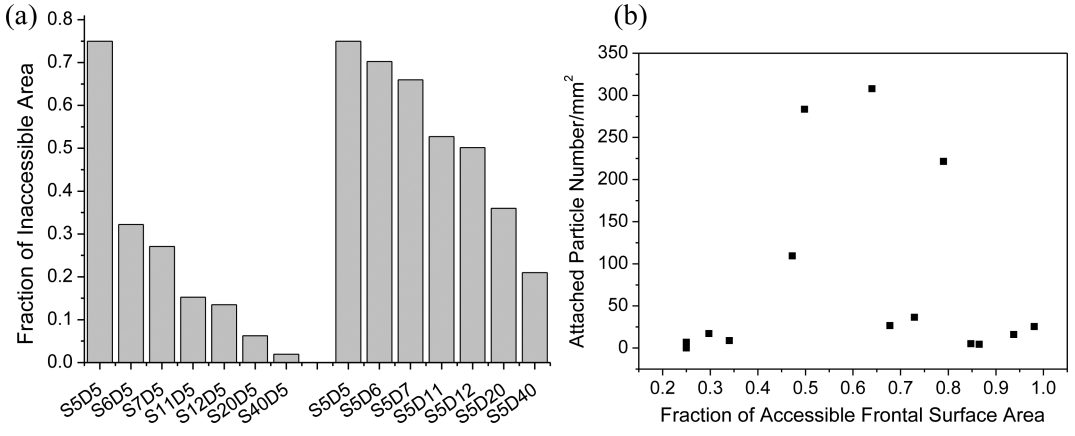

Figure 6. (a) Effect of surface patterning on area available for particle adhesion. (b) The number of particles attached as a function of accessible area.

dx.doi.org/10.1021/am500887w | ACS Appl. Mater. Interfaces 2014, 6, 8199–8207

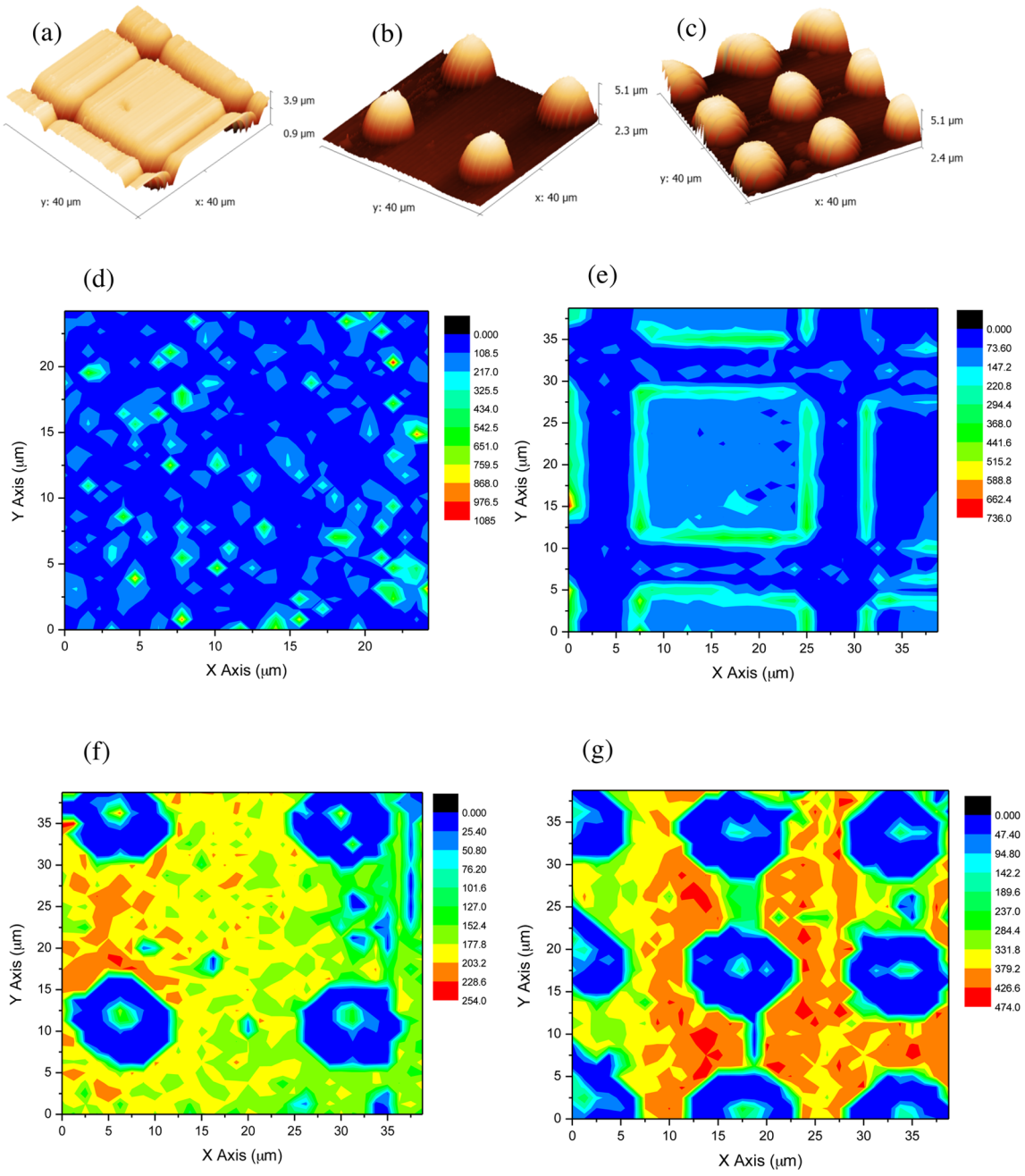

Figure 7. Surface morphology of pattern (a) pillar dimension = 20 μm, spacing = 5 μm; (b) pillar dimension = 5 μm, spacing = 20 μm; (c) pillar dimension = 5 μm, spacing = 12 μm; adhesion force spatial distribution contour on (d) smooth control; pattern (e) pillar dimension = 20 μm, spacing = 5 μm; (f) pillar dimension = 5 μm, spacing = 20 μm; (g) pillar dimension = 5 μm, spacing = 12 μm. Note: (1) different color scales are used in different force maps; (2) the pillars appear larger than the actual size due to the large size of the colloidal probe.

a second mode at higher adhesion force than that of 20 μm. This is attributed to the higher contact area when the particles are located in the valleys against the pillar walls (schematic in Figure S4b and c in Supporting Information), resulting in higher adhesion force (Figure 7g). The particles are geometrically more likely to interact with the walls in smaller accessible spacing comparing to larger spacing (schematic in Figure S4c in Supporting Information).

Another notable observation was that there were far more high adhesion force sites on the control surface than the patterned surfaces as shown by the long tail in the cumulative distribution of adhesion force. In addition, for patterns with the same small spacing of 5 μm, reducing pillar size seemed to eliminate high adhesion force sites.

The average and maximum adhesion forces as well as the number of particles attached on the surfaces compared in Figures 4, 7, and 8 are summarized in Table 1. It was clear that the average adhesion force was not a good indicator of particle adhesion (Figure S6 in Supporting Information) as it was notably larger on all patterned surfaces than on the smooth control surface. Despite the low mean adhesion force, the number of particles attached was the highest on the control surface. This is not surprising considering that the particles adhered only occupied a very small area of the surface, ranging from 0.01 to 1.17 % (Table 1). Such phenomenon suggests that

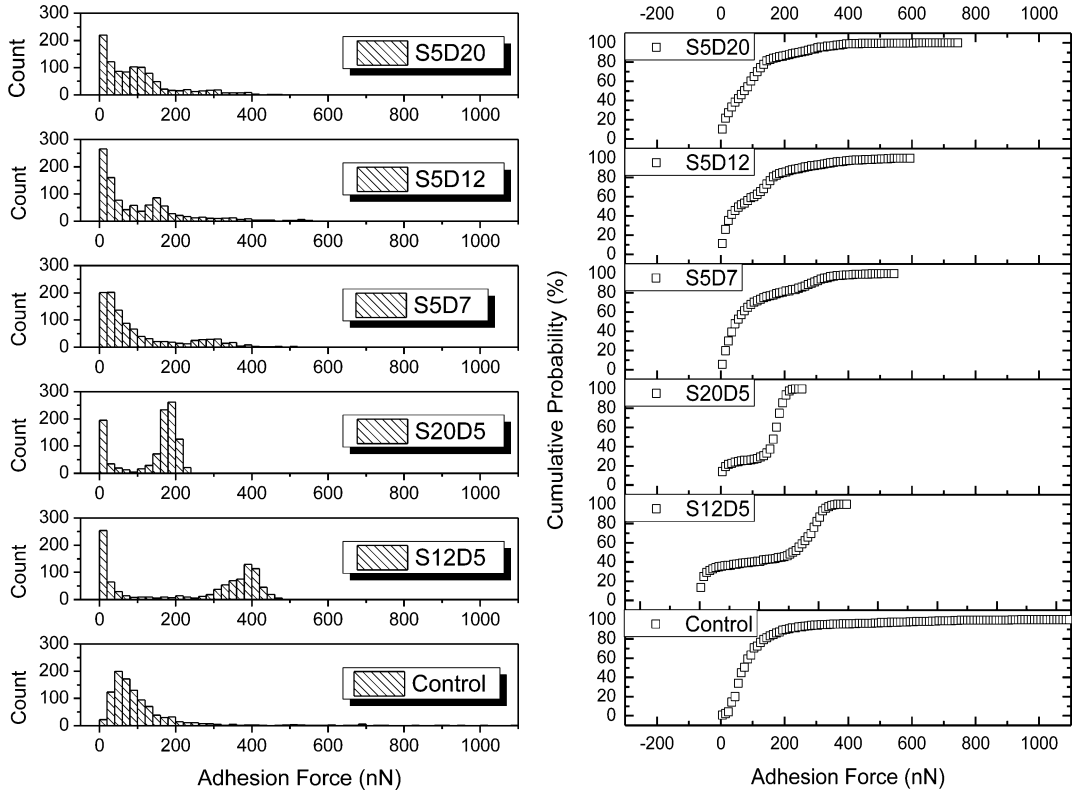

Figure 8. Frequency count and cumulative probability of adhesion force on selected patterns and smooth control surface.

Table 1. Measured Adhesion Force and Particle Attachment on the Control and Selected Pattern Surfaces

samples	avg. adhesion force[a] (nN)	max. adhesion force[a] (nN)	particles attached (/mm^2)	particle occupied area[b] (%)
control	72.3	1081.8	414	1.17
S12D5	232.8	472.8	3	0.01
S20D5	138.0	253.3	16	0.05
S5D7	103.1	519.2	9	0.03
S5D12	106.0	554.8	283	0.80
S5D20	101.8	735.0	308	0.87

[a]Scanning area: 40 μm × 40 μm on patterns, 25 μm × 25 μm on control. [b]Estimated as the attached particle number × particle projected area/frontal area of the surface.

a large area on the surface is either inaccessible to the particles or has insufficient adhesion forces for PSAA particle attachment under our experimental conditions. Particle adhesion seems to correlate better with the maximum adhesion force (Figure S6 in Supporting Information). On patterns with the same spacing of 5 μm and the smooth control surface, the number of particles attached increased monotonically with the maximum adhesion force. Considering that the smooth control surface has the highest maximum adhesion force and accessible area, these results suggest that the high adhesion force sites are responsible for the particle attachment observed. For patterns with small pillar dimensions (5 and 7 μm), particle attachment was extremely low and not correlating with either maximum or average adhesion forces, suggesting that other mechanisms may be more important. The AFM measurement does not provide information on hydrodynamics, which also plays an important role in particle attachment and is expected to be altered by surface patterns. Therefore, adhesion force alone may not be sufficient to completely explain particle adhesion behavior.

CONCLUSION

Although surface topography is known to play an important role in particle adhesion and fouling, its specific effects and the mechanisms involved are unclear. Using engineered surfaces with well-defined microscopic surface patterns, we successfully demonstrate that adhesion of micro-sized particles is strongly influenced by the size of and spacing between micro-scale pillar or pit features. Compared to the smooth control surface, all micro-patterns tested in our study greatly reduced particle adhesion. In general, particle adhesion decreased with decreasing surface feature size and spacing, but the effect was not related to the changes in available surface area. On pillared micro-patterns, there existed a critical pillar dimension similar to the particle diameter, below which particle adhesion was minimized. The pillared micro-patterns were found to strongly modulate the distribution of adhesion force on the surface, which in turn governed the distribution of particles on the surface. The presence of microscopic pillars created a bimodal distribution of the adhesion force, which was modulated by the dimension of and spacing between pillars. Our results also showed that the mean adhesion force on a patterned surface was not a good indicator for particle attachment as attachment only occurred at a small number of surface sites of very high adhesion forces. Overall, our findings suggest that surface patterning could be an attractive approach to manipulate surface adhesive properties and hence particle attachment. In addition to modulating surface adhesion forces, microscopic patterns could also influence particle attachment by altering hydrodynamic conditions near the surface. Further research on hydrodynamic conditions on a micro-patterned surface is

necessary to guide the design of micro-patterns for particle adhesion control.

■ ASSOCIATED CONTENT

Supporting Information

Pattern dimensions corresponding to Figures 2 and 3, ζ-potential of the PSAA particle at different pH, characterization of pattern surface vertical profile and surface chemistry, geometric analysis of available surface area, images of the AFM colloid probe used, and the correlation of adhesion force and attached particle number. This material is available free of charge via the internet at http://pubs.acs.org.

■ AUTHOR INFORMATION

Corresponding Author

*Email: qilin.li@rice.edu.

Present Address

[‖]J. Zhang: Gibson Applied Technology and Engineering, Inc., 16360 Park 10 Place, Suite 206, Houston, TX 77084

Author Contributions

The manuscript was written through contributions of all authors. All authors have given approval to the final version of the manuscript.

Notes

The authors declare no competing financial interest.

■ ACKNOWLEDGMENTS

We thank the financial support from the U.S. National Science Foundation (Awards CBET-1134427 and EEC-0647452), National Natural Science Foundation of China (Award 51228802), Air Force Office of Scientific Research (Award FA9550-13-1-0084), and Shell Center for Sustainability at Rice University.

■ REFERENCES

(1) Smith, M. J.; Kerr, A.; Cowling, M. J. Effects of Marine Biofouling on Gas Sensor Membrane Materials. *J. Environ. Monit.* **2007**, *9*, 1378–1386.

(2) Tang, C. Y. Y.; Chong, T. H.; Fane, A. G. Colloidal Interactions and Fouling of NF and RO Membranes: A Review. *Adv. Colloid Interface Sci.* **2011**, *164*, 126–143.

(3) Koo, C. H.; Mohammad, A. W.; Suja', F.; Meor Talib, M. Z. Review of the Effect of Selected Physicochemical Factors on Membrane Fouling Propensity Based on Fouling Indices. *Desalination* **2012**, *287*, 167–177.

(4) Ploux, L.; Ponche, A.; Anselme, K. Bacteria/Material Interfaces: Role of the Material and Cell Wall Properties. *J. Adhes. Sci. Technol.* **2010**, *24*, 2165–2201.

(5) Crawford, R. J.; Webb, H. K.; Truong, V. K.; Hasan, J.; Ivanova, E. P. Surface Topographical Factors Influencing Bacterial Attachment. *Adv. Colloid Interface Sci.* **2012**, *179-182*, 142–149.

(6) Anselme, K.; Davidson, P.; Popa, A. M.; Giazzon, M.; Liley, M.; Ploux, L. The Interaction of Cells and Bacteria with Surfaces Structured at the Nanometre Scale. *Acta Biomater.* **2010**, *6*, 3824–3846.

(7) Darbha, G. K.; Fischer, C.; Michler, A.; Luetzenkirchen, J.; Schafer, T.; Heberling, F.; Schild, D. Deposition of Latex Colloids at Rough Mineral Surfaces: An Analogue Study Using Nanopatterned Surfaces. *Langmuir* **2012**, *28*, 6606–6617.

(8) Nikkhah, M.; Edalat, F.; Manoucheri, S.; Khademhosseini, A. Engineering Microscale Topographies to Control the Cell–Substrate Interface. *Biomaterials* **2012**, *33*, 5230–5246.

(9) Jin, C.; Zhu, B.; Wang, X.; Lu, Q.; Chen, W.; Zhou, X. Nanoscale Surface Topography Enhances Cell Adhesion and Gene Expression of Madine Darby Canine Kidney Cells. *J. Mater. Sci.: Mater. Med.* **2008**, *19*, 2215–2222.

(10) Ploux, L.; Anselme, K.; Dirani, A.; Ponche, A.; Soppera, O.; Roucoules, V. Opposite Responses of Cells and Bacteria to Micro/Nanopatterned Surfaces Prepared by Pulsed Plasma Polymerization and UV-Irradiation. *Langmuir* **2009**, *25*, 8161–8169.

(11) Pan, Z.; Yan, C.; Peng, R.; Zhao, Y. C.; He, Y.; Ding, J. D. Control of Cell Nucleus Shapes Via Micropillar Patterns. *Biomaterials* **2012**, *33*, 1730–1735.

(12) Whitehead, K. A.; Colligon, J.; Verran, J. Retention of Microbial Cells in Substratum Surface Features of Micrometer and Sub-micrometer Dimensions. *Colloids Surf., B* **2005**, *41*, 129–138.

(13) Satriano, C.; Messina, G. M. L.; Carnazza, S.; Guglielmino, S.; Marletta, G. Bacterial Adhesion onto Nanopatterned Polymer Surfaces. *Mater. Sci. Eng.: C* **2006**, *26*, 942–946.

(14) Chung, K. K.; Schumacher, J. F.; Sampson, E. M.; Burne, R. A.; Antonelli, P. J.; Brennana, A. B. Impact of Engineered Surface Microtopography on Biofilm Formation of *Staphylococcus aureus*. *Biointerphases* **2007**, *2*, 89–94.

(15) Medilanski, E.; Kaufmann, K.; Wick, L. Y.; Wanner, O.; Harms, H. Influence of the Surface Topography of Stainless Steel on Bacterial Adhesion. *Biofouling* **2002**, *18*, 193–203.

(16) Hou, S. Y.; Gu, H. A.; Smith, C.; Ren, D. C. Microtopographic Patterns Affect *Escherichia coli* Biofilm Formation on Poly(dimethylsiloxane) Surfaces. *Langmuir* **2011**, *27*, 2686–2691.

(17) Allion, A.; Baron, J. P.; Boulange-Petermann, L. Impact of Surface Energy and Roughness on Cell Distribution and Viability. *Biofouling* **2006**, *22*, 269–278.

(18) Carman, M. L.; Estes, T. G.; Feinberg, A. W.; Schumacher, J. F.; Wilkerson, W.; Wilson, L. H.; Callow, M. E.; Callow, J. A.; Brennan, A. B. Engineered Antifouling Microtopographies—Correlating Wettability with Cell Attachment. *Biofouling* **2006**, *22*, 11–21.

(19) Hsu, L. C.; Fang, J.; Borca-Tasciuc, D. A.; Worobo, R. W.; Moraru, C. I. Effect of Micro- and Nanoscale Topography on the Adhesion of Bacterial Cells to Solid Surfaces. *Appl. Environ. Microbiol.* **2013**, *79*, 2703–2712.

(20) Graham, M. V.; Mosier, A. P.; Kiehl, T. R.; Kaloyeros, A. E.; Cady, N. C. Development of Antifouling Surfaces to Reduce Bacterial Attachment. *Soft Matter* **2013**, *9*, 6235–6244.

(21) Perni, S.; Prokopovich, P. Micropatterning with Conical Features Can Control Bacterial Adhesion on Silicone. *Soft Matter* **2013**, *9*, 1844–1851.

(22) Scheuerman, T. R.; Camper, A. K.; Hamilton, M. A. Effects of Substratum Topography on Bacterial Adhesion. *J. Colloid Interface Sci.* **1998**, *208*, 23–33.

(23) Hoek, E. M. V.; Agarwal, G. K. Extended DLVO Interactions between Spherical Particles and Rough Surfaces. *J. Colloid Interface Sci.* **2006**, *298*, 50–58.

(24) Hoek, E. M. V.; Bhattacharjee, S.; Elimelech, M. Effect of Membrane Surface Roughness on Colloid/Membrane DLVO Interactions. *Langmuir* **2003**, *19*, 4836–4847.

(25) Suresh, L.; Walz, J. Y. Effect of Surface Roughness on the Interaction Energy between a Colloidal Sphere and a Flat Plate. *J. Colloid Interface Sci.* **1996**, *183*, 199–213.

(26) Martines, E.; Csaderova, L.; Morgan, H.; Curtis, A. S. G.; Riehle, M. O. DLVO Interaction Energy between a Sphere and a Nanopatterned Plate. *Colloid Surf., A* **2008**, *318*, 45–52.

(27) Curtis, A. S. G.; Wilkinson, C. D. Reactions of Cells to Topography. *J. Biomater. Sci., Polym. Ed.* **1998**, *9*, 1313–1329.

(28) Rizzello, L.; Sorce, B.; Sabella, S.; Vecchio, G.; Galeone, A.; Brunetti, V.; Cingolani, R.; Pompa, P. P. Impact of Nanoscale Topography on Genomics and Proteomics of Adherent Bacteria. *ACS Nano* **2011**, *5*, 1865–1876.

(29) Diaz, C.; Salvarezza, R. C.; de Mele, M.; Schilardi, P. L. Organization of *Pseudomonas fluorescens* on Chemically Different Nano/Microstructured Surfaces. *ACS Appl. Mater. Interfaces* **2010**, *2*, 2530–2539.

(30) Schneider, C. A.; Rasband, W. S.; Eliceiri, K. W. NIH Image to ImageJ: 25 Years of Image Analysis. *Nat. Methods* **2012**, *9*, 671–675.

(31) Tortonese, M.; Kirk, M. Characterization of Application Specific Probes for SPMs. *Proc. SPIE 3009, Micromachining and Imaging (April 15, 1997)* **1997**, DOI: 10.1117/12.271229.
(32) Callow, M. E.; Jennings, A. R.; Brennan, A. B.; Seegert, C. E.; Gibson, A.; Wilson, L.; Feinberg, A.; Baney, R.; Callow, J. A. Microtopographic Cues for Settlement of Zoospores of the Green Fouling *Alga enteromorpha*. *Biofouling* **2002**, *18*, 237−245.